Design of a Polymer Directional Coupler Electro-Optic Switch with Low Push-Pull Switching Voltage at 1550nm*

Zheng Chuantao, Ma Chunsheng†, Yan Xin, Wang Xianyin, and Zhang Daming

(*State Key Laboratory of Integrated Optoelectronics, College of Electronic Science and Engineering, Jilin University, Changchun* 130012, *China*)

Abstract: A polymer directional coupler (DC) electro-optic switch with push-pull electrodes and rib waveguides is designed based on the conformal transforming method, image method, coupled mode theory, and electro-optic modulation theory. Its structure and principle are described, the design and optimization are performed, and the characteristics are analyzed, including the coupling length, switching voltage, output power, insertion loss, and crosstalk. To realize normal switching function, the fabrication tolerance, wavelength shift, and coupling loss between a single mode fiber (SMF) and the waveguide are discussed. Simulation results show that the coupling length is 3082μm; the push-pull switching voltage is 2.14V; and the insertion loss and crosstalk are less than 1.14 and -30dB, respectively. The proposed analytical technique on waveguides and electrodes is proven to be accurate and computationally efficient when compared with the beam propagation method (BPM) and the experimental results.

Key words: electro-optic switch; push-pull electrodes; coupling length; switching voltage; insertion loss; crosstalk
EEACC: 4150
CLC number: TN253 **Document code**: A **Article ID**: 0253-4177(2008)11-2197-07

1 Introduction

With the development of the optical communication technology, information transmission capacity is increasing gradually. In order to meet the need for high speed and large capacity, it has become an unavoidable trend to replace electrical devices and exchange with optical devices and exchange. Optical switches and their arrays have become key components in optical cross-connects (OXC), optical add-drop multiplexers (OADM), and optical line protection (OLP), because of their applications in optical signal processing, optical computers, and optical instruments, equipment, and sensors. Therefore, they have become a hot research issue home and abroad, and great progress has been made recently[1~4]. Optical switches should be designed and fabricated with excellent features including low switching voltage, short switching time, fast switching speed, high extinction ratio, low insertion loss, and low crosstalk, which has become an urgent task nowadays. Polymer electro-optic materials possess high electro-optic coefficients, low transmission loss, fast response speed, easy control of refractive index, and simple technology in processing. Therefore, they are widely used to fabricate optical switches and modulators[5~8]. Recently, a novel hybrid polymer material with a high electro-optic coefficient has been used to fabricate modulators with good performances[9,10] and it is also used in this paper.

In this paper, relying on the conformal transforming method[11], image method[12], coupled mode theory, and electro-optic modulation theory, a polymer directional coupler electro-optic switch with rib waveguides and push-pull electrodes is proposed. Its structure and principle are described, and the technique and relative formulas are presented. The parameters are optimized, including the core width, core thickness, rib height, buffer layer thickness, and coupling gap. Characteristics are analyzed, involving the transmission spectrum, operation voltage, insertion loss, crosstalk, fabrication tolerance, and wavelength shift. The coupling loss between an SMF and the waveguide is also calculated by the finite-difference beam propagation method (FD-BPM).

2 Model and theory

2.1 Model of the switch

Figure 1 shows the structural schematic picture of

* Project supported by the National Natural Science Foundation of China (No. 60706011), the Doctoral Program for New Teachers of the Ministry of Education of China (No. 20070183087), and the State Key Development Program for Basic Research of China (No. 2006CB302803)
† Corresponding author. Email: mcsheng@163.com
Received 15 April 2008, revised manuscript received 22 June 2008

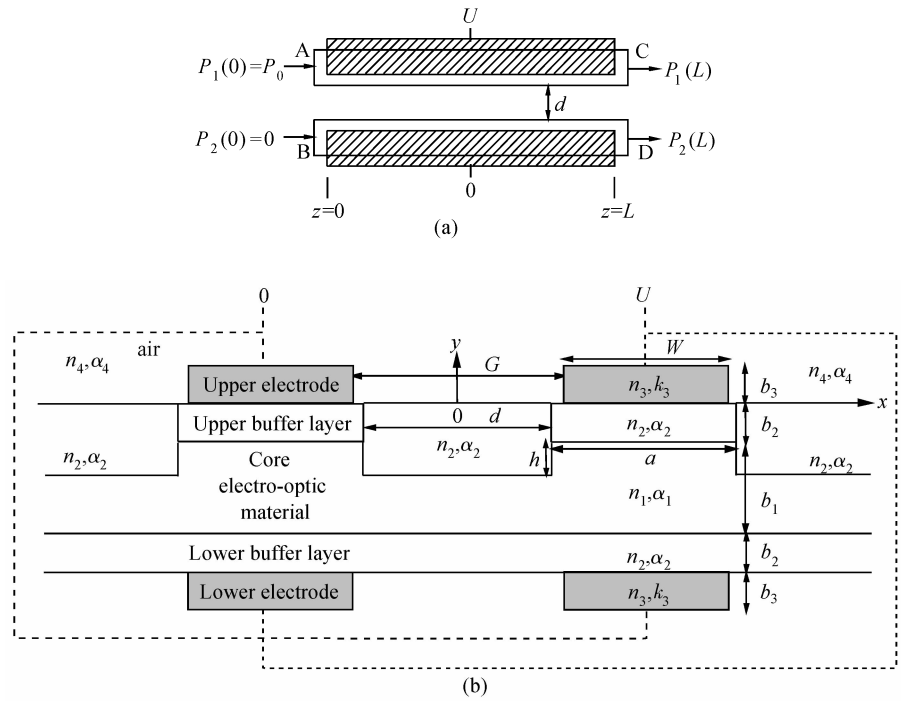

Fig. 1 Structural diagram (a) and cross-section (b) with operation voltage U of a polymer directional coupler electro-optic switch with push-pull electrodes

the polymer directional coupler electro-optic switch, which consists of two identical parallel rib waveguides. The coupling region is shown in Fig. 1 (a), where d is the coupling gap between the waveguides and L is the length of the coupling region. The structure of the rib waveguide is given as: air/upper electrode/upper buffer layer/core/lower buffer layer/lower electrode/substrate, as shown in Fig. 1(b), where only the core is electro-optic material. In order to pole the electro-optic polymer core material and operate the device, a push-pull electrode structure is adopted, which consists of a pair of upper electrodes and a pair of lower electrodes. During poling, the applied poling voltages on the top two electrodes should be U_{pol}, while those on the lower electrodes should be 0; during operation, the applied operation voltage U is shown in Fig. 1(b).

We denote W and G as the electrode width and gap, respectively, and let a be the core width, b_1 be the core thickness, h be the rib height, n_1 be the core refractive index, and α_1 be its bulk loss coefficient. We let b_2 be the thickness of the upper/lower buffer layers, n_2 be the refractive index of the upper/lower buffer layers and the cladding beside the rib, and α_2 be their bulk loss coefficient. We let b_3 be the thickness of the upper/lower electrodes, n_3 be its refractive index, and κ_3 be its bulk extinction coefficient. We let n_4 be the refractive index of the cladding above the upper electrode, and α_4 be its bulk loss coefficient.

2.2 Electrode analysis

The electric field in each waveguide along the y-direction produced by the push-pull electrode structure can be divided into three parts: one is uniform caused by the up-down electrodes, denoted by $E_{1y}(x, y)$, and the other two are non-uniform caused by the two upper coplanar electrodes and the two lower coplanar electrodes, denoted by $E_{2y}(x, y)$ and $E_{3y}(x, y)$, respectively. According to the electric-magnetic field theory, we can obtain $E_{1y}(x, y)$ as:

$$E_{1y}(x, y) = \frac{n_2^2 U}{2n_1^2 b_2 + n_2^2 b_1} \tag{1}$$

The two upper coplanar electrodes shown in Fig. 1(b) can be mapped into a parallel electrode structure along the y-direction. When the electrodes are directly on the core, which means that no buffer layer exists between the core and the electrodes, $b_2 = 0$, then the electric field along the y-direction can be expressed as[11]:

$$E_{20,y}(x, y) = \frac{U}{2K'} \operatorname{Im} \frac{\mathrm{d}w}{\mathrm{d}z} \tag{2}$$

where $\dfrac{\mathrm{d}w}{\mathrm{d}z} = \dfrac{g}{\sqrt{(g^2 - k^2 z^2)(g^2 - z^2)}}$, $g = \dfrac{G}{2}$, $k = \dfrac{G}{G + 2W}$. Let $K' = F(\pi/2, k)$ be the first ellipse integral. When a buffer layer exists between the core and the electrode, $b_2 \neq 0$, we can get the electric field in the waveguides by the image method[12] as:

$$E_{2y}(x, y) = (1 - r) \sum_{v=0}^{\infty} r^v E_{20,y}(x, y + 2vb_2) \tag{3}$$

where $r = \frac{n_1^2 - n_2^2}{n_1^2 + n_2^2}$ is the reflection coefficient, and $E_{20,y}(x,y)$ can be calculated from Eq.(2). Similarly, the electric field in the y-direction caused by the two under coplanar electrodes $E_{3y}(x,y)$ can be expressed as

$$E_{3y}(x,y) = E_{2y}(x, -b_1 - 2b_2 - y) \tag{4}$$

Then, the total electric field along the y-direction in each waveguide can be written as

$$E_y(x,y) = E_{1y}(x,y) + E_{2y}(x,y) + E_{2y}(x, -b_1 - 2b_2 - y) \tag{5}$$

In order to describe the electro-optic modulation efficiency, we introduce the overlap integral in the y-direction as

$$\Gamma_y = G \frac{\iint \frac{1}{U} E_y(x,y) \, |E'(x,y)|^2 \mathrm{d}x\mathrm{d}y}{\iint |E'(x,y)|^2 \mathrm{d}x\mathrm{d}y} \tag{6}$$

where $E'(x,y)$ is the mode optical field distribution, and the integral is over the electro-optic interaction coupling region. From Eqs.(1), (2), (4), and (5), we can get the expression $E_y(x,y)/U$, then the overlap integral Γ_y can be obtained from Eq.(6).

2.3 Switching function

Under the operation voltage U, based on electro-optic modulation theory, the change of the refractive index of one waveguide core caused by the applied voltage can be determined by

$$\Delta n_1 = \frac{n_1^3}{2} \gamma_{33} \frac{U}{G} \Gamma_y \tag{7}$$

We let β_1, β_2 be the mode propagation constants of the two waveguides and let $2\delta = \beta_2 - \beta_1$. Based on coupled mode theory, the propagation powers in waveguide 1 and 2 are, respectively,

$$P_{10}(z) = \frac{P_0}{\delta^2 + K^2} \{(\delta^2 + K^2)\cos^2[(\delta^2 + K^2)^{1/2} z] + \delta^2 \sin^2[(\delta^2 + K^2)^{1/2} z]\} \tag{8a}$$

$$P_{20}(z) = \frac{P_0}{\delta^2 + K^2} K^2 \sin^2[(\delta^2 + K^2)^{1/2} z] \tag{8b}$$

where K is the coupling coefficient.

When no voltage is applied on the electrode, i.e. $U = 0$, the mode propagation constants of the two waveguides will be identical, which means $\beta_1 = \beta_2 \equiv \beta$, then $\delta = 0$. To enable the input power of waveguide 1 entirely output from waveguide 2, i.e. $P_{10}(L) = 0$, $P_{20}(L) = P_0$, according to Eqs.(8a) and (8b), the coupling region length L should be

$$L = (2m + 1)L_0, \quad m = 0, 1, 2, \cdots \tag{9}$$

where $L_0 = \pi/2K$, which is the coupling length. So L can be taken as $L = L_0$.

For the case of $U \neq 0$, $\beta_1 \neq \beta_2$, and $\delta \neq 0$, when the coupling region length L is taken to be L_0, to enable the input power of waveguide 1 still entirely output from waveguide 1, i.e. $P_{10}(L_0) = P_0$, $P_{20}(L_0) = 0$, from Eqs.(8a) and (8b), we get $\delta = \sqrt{3}K = \sqrt{3}\pi/2L_0$. In this case, the switching function is realized in the device, and the relative operation voltage is called the switching voltage, denoted by U_s.

When the mode loss is considered, the mode propagation constant β will be changed to $\beta - \mathrm{j}\alpha$, where α is the mode loss coefficient, and the output powers of the two waveguides should be rewritten as

$$P_1(z) = P_{10}(z)\exp(-2\alpha z)$$
$$P_2(z) = P_{20}(z)\exp(-2\alpha z) \tag{10}$$

where $P_{10}(z)$ and $P_{20}(z)$ are given by Eqs.(8a) and (8b).

3 Simulation results and discussion

We select the operation wavelength in free space $\lambda_0 = 1550\mathrm{nm}$. The refractive index of the core $n_1 = 1.643$, its bulk loss coefficient $\alpha_1 = 2.0\mathrm{dB/cm}$, and its electro-optic coefficient $\gamma_{33} = 138\mathrm{pm/V}$[9,10]; the refractive index of the buffer layer and cladding beside the core $n_2 = 1.461$, and its bulk loss coefficient $\alpha_2 = 0.25\mathrm{dB/cm}$[13]; the electrode is made of aurum, its refractive index $n_3 = 0.19$, and its bulk extinction coefficient $\kappa_3 = 6.1$[14]. The layer upon the electrodes is air, its refractive index $n_4 = 1.0$, and its bulk loss coefficient $\alpha_4 = 0$. Here, we take the electrode width W and electrode gap G as the core width a and the waveguide gap d, respectively. We select E_{00}^x mode propagating in the device. According to the theory and formulas presented in this paper, calculation programs based on MATLAB are compiled, and simulation results are given as follows.

3.1 Thickness of electrode and buffer layer

Figure 2 shows the effects of the buffer thickness b_2 and electrode thickness b_3 on the mode effective refractive index n_{eff} and mode loss coefficient α. First, we take the electrode thickness $b_3 = 100\mu\mathrm{m}$, which can be regarded as infinite. We find that, when $b_2 \geqslant 1.5\mu\mathrm{m}$, n_{eff} and α become constants, respectively, and the mode propagation and mode loss will form a steady state. Then the propagation constants of the parts of the waveguide with/without the electrode will be identical, and the coupling loss will be decreased as small as possible. On the other hand, to increase the electric field in the core, b_2 cannot be too large. So we select $b_2 = 1.5\mu\mathrm{m}$.

However, b_3 cannot be infinite in fabrication, so the minimum electrode thickness should be decided. Figure 2(b) shows that, when b_3 increases large enough, n_{eff} and α become constants, respectively, and the mode propagation and mode loss will also form a

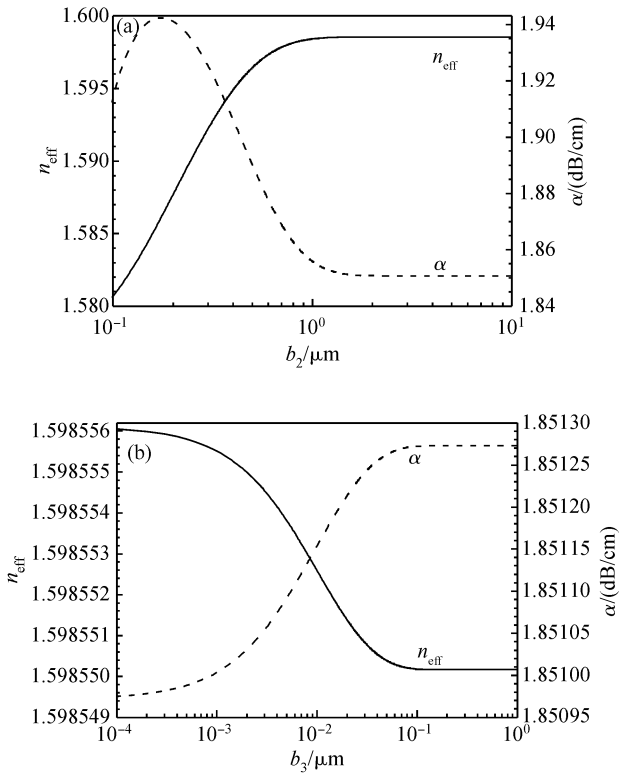

Fig. 2 Effects of the buffer layer thickness b_2 (a) and electrode thickness b_3 (b) on the mode effective refractive index n_{eff} and mode loss coefficient α, where $U = 0$, $a = 4.0\mu m$, $b_1 = 1.5\mu m$, $h = 0.5\mu m$, (a) $b_3 = 100\mu m$, and (b) $b_2 = 1.5\mu m$

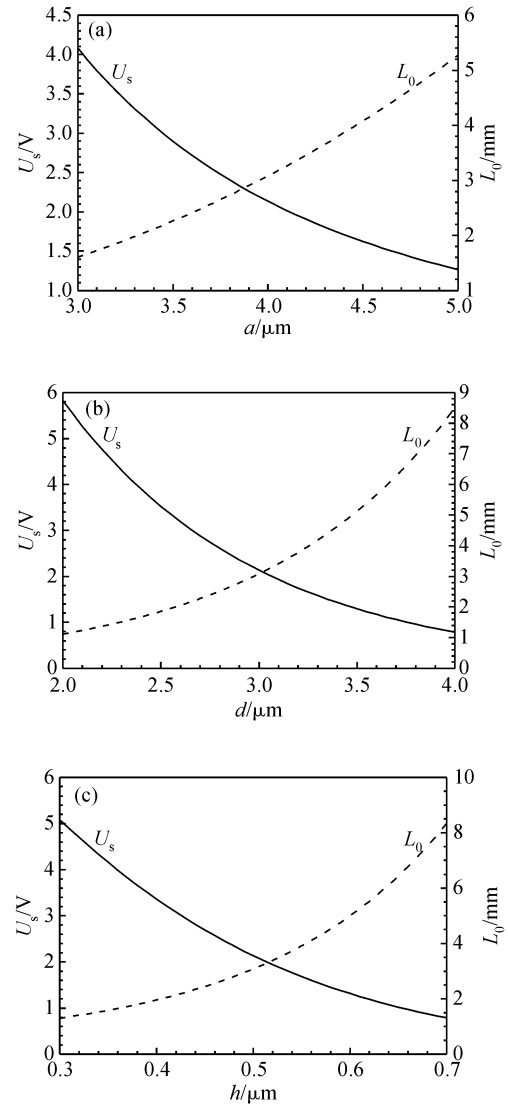

Fig. 3 Effects of the core width a (a), coupling gap d (b), and rib height h (c) on the coupling length L_0 and switching voltage U_s, where $b_1 = 1.5\mu m$, $b_2 = 1.5\mu m$, $b_3 = 0.10\mu m$, $W = a$, $G = d$, (a) $h = 0.5\mu m$, $d = 3.0\mu m$, (b) $a = 4.0\mu m$, $h = 0.5\mu m$, and (c) $a = 4.0\mu m$, $d = 3.0\mu m$

steady state. When $b_3 \geqslant 0.1\mu m$, the electrodes can be regarded as sufficiently large, which agrees with the assumption of $b_3 = 100\mu m$ in Fig. 2(a). Considering all the influences of b_2 and b_3 on n_{eff} and α, we select $b_2 = 1.5\mu m$ and $b_3 = 0.1\mu m$. In this case, the mode amplitude loss coefficient is $\alpha = 1.85$dB/cm, which will be taken into account in the following simulation.

3.2 Core width, coupling gap and rib height

Figure 3 shows the effects of the core width a, coupling gap d, and rib height h on the coupling length L_0 and switching voltage U_s. This figure shows that when a, d, or h increases, L_0 increases while U_s decreases. Summarizing all the effects caused by a, d, and h, we select $a = 4.0\mu m$, $b_1 = 1.5\mu m$, $h = 0.5\mu m$, and $d = 3.0\mu m$; in this case, the coupling length L_0 is about $3082\mu m$, and the switching voltage U_s is about 2.14V. These parameters also assure the single mode waveguide.

3.3 Simulation of switching characteristics

Figure 4 plots the curves of output powers P_1 and P_2 versus the coupling region length L. Figure 4(a) shows that, under the operation voltage of $U = 0$, when the coupling region length L is taken to be odd times of L_0, P_1 becomes the minimum, while P_2 becomes the maximum. Figure 4(b) shows that, under the operation voltage of $U_s = 2.14$V, when the coupling region length L is taken to be the integer times of the coupling length L_0, P_1 becomes the maximum, while P_2 becomes the minimum.

Figure 5 presents the curves of output powers P_1 and P_2 versus the applied voltage U, where we take $L = L_0, 3L_0$. From the results, we find that U_s decreases as L_0 increases with the odd times. The switching voltage is 2.14V when $L = L_0$, while it is 1.09V when $L = 3L_0$. Therefore, in the design of such a device, the switching voltage can be decreased greatly by increasing the coupling region length within the permitted integration.

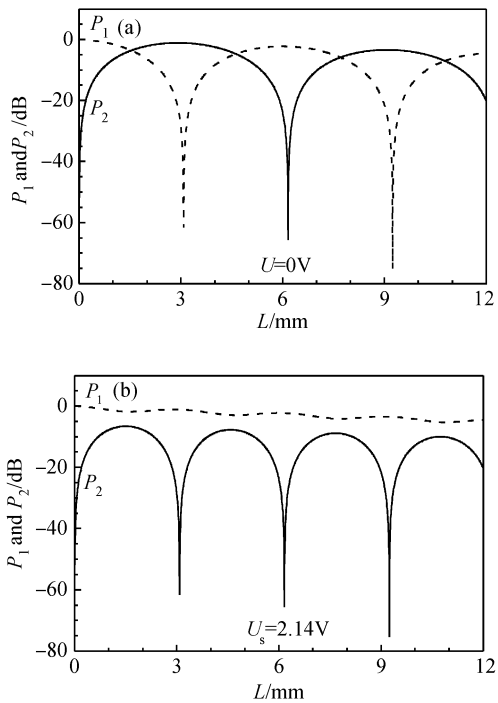

Fig. 4　Curves of the output powers P_1 and P_2 versus the coupling region length L, where $a = 4.0\mu$m, $b_1 = 1.5\mu$m, $h = 0.5\mu$m, $d = 3.0\mu$m, (a) $U = 0$ and (b) $U = U_s$

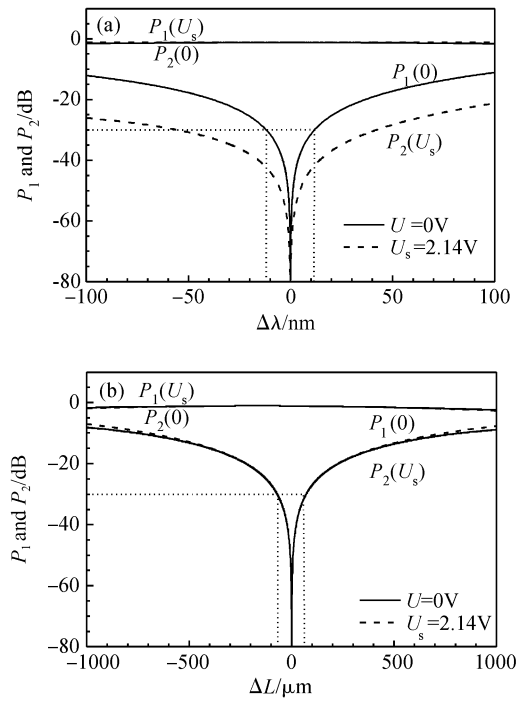

Fig. 6　Effects of the error of the wavelength shift Δλ (a) and the coupling region length ΔL (b) on the output powers P_1 and P_2, where $a = 4.0\mu$m, $b_1 = 1.5\mu$m, $h = 0.5\mu$m, $d = 3.0\mu$m, and $U = 0, U_s$

3.4　Fabrication tolerance and wavelength shift

The device will have excellent switching features when the coupling region length L is exactly equal to L_0. However, the fabrication error of the coupling region length exists inevitably, which will affect the performance of the device. Moreover, during the operation of the device, it is difficult to keep the practical operation wavelength λ exactly equal to the designed operation wavelength λ_0, which will also affect the performance of the device. Figure 6 shows the effects of the wavelength shift $\Delta\lambda$ and the error of the coupling region length ΔL on the output powers P_1 and P_2, where we take the operation voltage $U = 0$ and $U_s = 2.14$V. Figure 6(a) shows that, in the range $-12\text{nm} \leqslant \Delta\lambda \leqslant 12\text{nm}$ (the relative range of the wavelength is $1538\text{nm} \leqslant \lambda \leqslant 1562\text{nm}$), the insertion loss and crosstalk are less than 1.14 and −30dB, respectively. Figure 6(b) shows that in the range $-70\mu\text{m} \leqslant \Delta L \leqslant 70\mu\text{m}$ (the relative range of the coupling region length is $3012\mu\text{m} \leqslant L \leqslant 3152\mu\text{m}$), the insertion loss and crosstalk are less than 1.17 and −30dB, respectively.

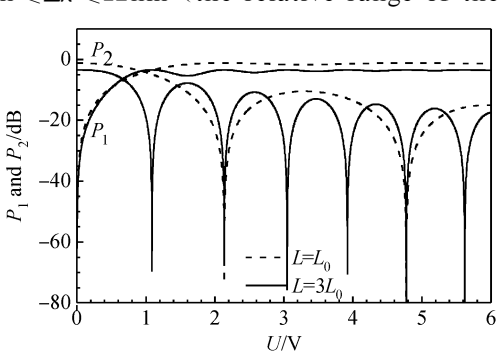

Fig. 5　Curves of the output powers P_1 and P_2 versus the applied voltage U, where $a = 4.0\mu$m, $b_1 = 1.5\mu$m, $h = 0.5\mu$m, $d = 3.0\mu$m, and $L = L_0, 3L_0$

3.5　Coupling loss with SMF

The coupling between the optical fiber and the waveguide is a key step of device packaging and directly affects the insertion loss of the device. The coupling loss between the SMF and the waveguide is caused by the following factors: the reflection of the coupling interface, the dislocation, gap, angle, and mode mismatch between the fiber and the waveguide, of which the main factor is the mode mismatch. To analyze the coupling loss of the designed switch with a standard SMF whose core radius is about 4μm, we calculate the coupling loss using FD-BPM. By considering the difference of the mode field diameter between the SMF and the switch only, the coupling loss of one waveguide with SMF is about 0.8 ~ 1.0dB. Considering possible coupling losses produced by the other factors, the total loss is less than 2dB, which is close to the result of our experiment.

3.6　Check of this design technique

In order to check the accuracy of the proposed

Table 1 Comparative study of results from our design technique with those from BPM

DC switch (this paper)	Switching voltage /V	Coupling length /μm
Our technique	2.14	3082
BPM	2.04	3240
Relative error	+4.9%	−4.8%

Table 2 Comparative study of results from our design technique with those from experiment

DC modulator & switch	Switching voltage /V	Coupling length /cm
Our technique	3.59	1.76
Experimental results[15]	3.60	1.80
Relative error	−0.3%	−2.2%

(Relative values of parameters: rib core width: 4.0μm, core thickness: 2.0μm, rib height: 0.3μm, upper/under cladding thickness: 3.0μm, electrode thickness: 0.2μm, coupling gap: 6.0μm, refractive index of the EO polymer and the cladding: 1.62@1.31μm, 1.54@1.31μm)

technique, a comparison is performed between the simulated results of this technique and those of the BPM for the designed switch, which are listed in Table 1. We conclude that they are in good agreement. Furthermore, this technique can also be used for the 1×2 Y-fed directional coupler modulator. A comparison is also carried out between our simulated results and the experimental results reported in Ref. [15], which are listed in Table 2. This confirms that this technique possesses high accuracy. The preceding comparisons indicate that this technique can be applied to the engineering design of these kinds of switches and modulators.

4 Conclusion

A polymer directional coupler electro-optic switch with push-pull electrodes and rib waveguides is simulated and optimized using the conformal transforming method, image method, coupled mode theory, and electro-optic modulation theory. Under the operation wavelength of 1550nm, the optimized values of the parameters are: the core width is 4.0μm, core thickness is 1.5μm, rib height is 0.5μm, the upper/under buffer layer thickness is 1.5μm, the coupling gap is 3.0μm, and the upper/lower electrode thickness is 0.1μm. In this case, the push-pull switching voltage is 2.14V, and the coupling length is 3082μm. Within the range of the operation wavelength from 1538 to 1562nm, the insertion loss and crosstalk are less than 1.14 and −30dB, respectively; Within the range of the coupling region length from 3012 to 3152μm, those are less than 1.17 and −30dB, respectively. These results show that the device designed in this paper possesses favorable switching functions.

References

[1] Suzuki K, Yamada T, Ishii M, et al. High-speed optical 1×4 switch based on generalized Mach-Zehnder interferometer with hybrid configuration of silica-base PLC and lithium niobate phase-shifter array. IEEE Photonics Technol Lett, 2007, 19(9～12): 674

[2] Tian Y, Xiao X S, Gao S M, et al. All-optical switch based on two-pump four-wave mixing in fibers without a frequency shift. Appl Opt, 2007, 46(23): 5588

[3] Lin Y Y, Lin S T, Chang G W, et al. Electro-optic periodically poled lithium niobate Bragg modulator as a laser Q-switch. Opt Lett, 2007, 32(5): 545

[4] Chen Zhiwen, Li Baojun, Chaudhari B S, et al. A 2×3 photonic switch in SiGe for 1.55μm operation. Chinese Journal of Semiconductors, 2006, 27(3): 494

[5] Gardelein A, Le Tacon S, Tanguy E, et al. Passive electro-optic antenna using polymer material. Electron Lett, 2007, 43(9): 489

[6] Swamy R, Rajagopalan H, Vippa P, et al. Quadratic electro-optic effect in a nano-optical material based on the nonconjugated conductive polymer, poly(ethylenepyrrolediyl) derivative. Solid State Commun, 2007, 143(11/12): 519

[7] Lu Fei, Liang Kun, Song Qiong, et al. Traveling-wave electrodes for polymer electro-optic modulator. Chinese Journal of Optoelectronics · Laser, 2005, 16(3): 267

[8] Liang Kun, Chen Wang, Wu Boyu, et al. Polymeric thermo-optic digital optical switches. Chinese Journal of Semiconductors, 2006, 27(4): 747

[9] Enami Y, Derose C T, Mathine D, et al. Hybrid polymer/sol-gel waveguide modulators with exceptionally large electro-optic coefficients. Nature Photonics, 2007, 1(3): 180

[10] Enami Y, Derose C T, Norwood R A. Hybrid cross-linkable polymer/sel-gel waveguide modulators with 0.65V half wave voltage at 1550nm. Appl Phys Lett, 2007, 91(9): 093505

[11] Ramer O G. Integrated optic electrooptic modulator electrode analysis. IEEE J Quantum Electron, 1982, 18(3): 386

[12] Sabatier C, Caquot E. Influence of a dielectric buffer layer on the field distribution in an electrooptic guided-wave device. IEEE J Quantum Electron, 1986, 18(1): 32

[13] Pitois C, Vukmirovic C, Hult A. Low-loss passive optical waveguides based on photosensitive poly(pentafluorostyrene-co-glycidyl methacrylate). Macromolecules, 1999, 32(9): 2903

[14] Driscoll W G, Vaughan W. Handbook of optics. New York: McGraw-Hill, 1978: 7

[15] An Dechang, Shi Zan, Sun Lin, et al. Polymeric electro-optic modulator based on 1×2 Y-fed directional coupler. Appl Phys Lett, 2000, 76(15): 1972

1550nm 低推挽电压聚合物定向耦合电光开关的设计*

郑传涛　马春生†　闫　欣　王现银　张大明

（吉林大学电子科学与工程学院 集成光电子学国家重点联合实验室吉林大学试验区，长春　130012）

摘要：应用保角变换法、镜像法、耦合模理论和电光调制理论设计了一种推挽电极聚合物脊形波导定向耦合电光开关，阐述了基本结构和工作原理，给出了器件的设计和优化过程，主要分析了耦合长度、开关电压、输出光功率、插入损耗、串扰等特性.为了实现正常的开关功能，讨论了制作公差、波谱漂移以及单模光纤耦合损耗对器件性能的影响.模拟结果表明，所设计的开关的耦合长度为3082μm，开关电压为 2.14V；插入损耗小于 1.14dB，串扰小于 －30dB.与 BPM 仿真结果以及实验结果的对比表明，文中提出的波导和电极的理论分析与计算方法具有较高的精度和可行性.

关键词：电光开关；推挽电极；耦合长度；开关电压；插入损耗；串扰

EEACC：4150

中图分类号：TN253　　**文献标识码**：A　　**文章编号**：0253-4177(2008)11-2197-07

* 国家自然科学基金（批准号：60706011），教育部博士点新教师基金（批准号：20070183087）及国家重点基础研究发展规划（批准号：2006CB302803）资助项目

† 通信作者.Email：mcsheng@163.com

2008-04-15 收到，2008-06-22 定稿